Enhancing Photovoltage of Silicon Photoanodes by a High Work-Function Coordination Polymer

Ponart Aroonratsameruang, Kanokwan Klahan, Gabriel Loget, Pichaya Pattanasattayavong

Enhancing Photovoltage of Silicon Photoanodes by a High Work-function Coordination Polymer

Ponart Aroonratsameruang,[†] Kanokwan Klahan,[†] Gabriel Loget,[‡]

Pichaya Pattanasattayavong*[,†,§]

[†]Department of Materials Science and Engineering, School of Molecular Science and Engineering, Vidyasirimedhi Institute of Science and Technology (VISTEC), Rayong, 21210, Thailand.

[‡]Univ Rennes, CNRS, ISCR (Institut des Sciences Chimiques de Rennes)-UMR6226, F-35000 Rennes, France.

[§]Research Network of NANOTEC-VISTEC on Nanotechnology for Energy, Vidyasirimedhi Institute of Science and Technology (VISTEC), Rayong, 21210, Thailand

Corresponding Author

*Email: pichaya.p@vistec.ac.th

ABSTRACT

A metal-insulator-semiconductor (MIS) structure based on an inhomogeneous junction has been recently proven to be highly efficient at photoelectrochemical (PEC) water oxidation. Engineering the surrounding layer of the MIS nanojunction is crucial to maximize the photovoltage. Specifically, for an n-type photoanode, a high work-function material is desired to create a large Schottky barrier that assists the hole transfer to oxidize water while blocking the electron transfer. We demonstrate the use of copper(I) thiocyanate (CuSCN), a transparent p-type coordination polymer semiconductor with a high work function, to surround the n-Si/SiO_x/Cu nanojunctions, resulting in an increased effective barrier height from 0.71 to 1.03 eV. This phenomenon, known as the pinch-off effect, is also applied to improve the performance of the planar n-Si/SiO_x/Cu electrode via a PEC dissolution method that creates an inhomogeneous surface covered with CuO_x. The Cu/CuSCN nanojunction still shows superior performance due to the favorable energetics of CuSCN.

TOC GRAPHICS

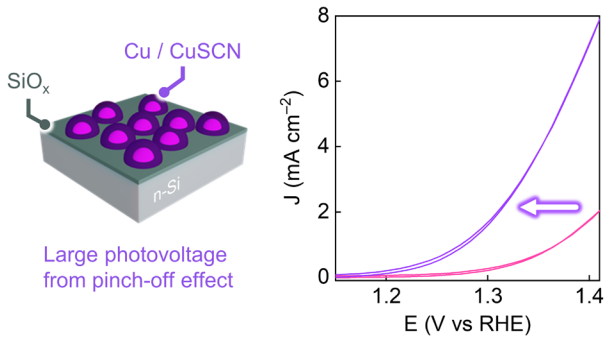

KEYWORDS: photoelectrochemical water splitting, silicon photoanodes, metal-insulator-semiconductor junctions, copper(I) thiocyanate, photovoltage

Harvesting sunlight by photoelectrochemical (PEC) reactions allows the long-term storage of solar energy in the form of stable chemical products, such as H_2 and O_2 through PEC water splitting reactions in the simplest case.[1,2] To drive the oxygen evolution reaction (OER), an excellent photoanode is required to overcome the high thermodynamic potential [$E^0_{O_2/H_2O}$ = 1.23 V vs reversible hydrogen electrode (RHE)].[3,4] Si, with a narrow band gap of 1.1 eV, has been demonstrated as a prominent candidate for driving uphill electrochemical reactions, e.g., water reduction,[5] CO_2 reduction,[6,7] and N_2 reduction.[8] The merits of Si also include the well-established infrastructure based on microelectronic/photovoltaic industries that could allow rapid scaling-up and deployment.[9] However, Si suffers from its poor OER activity and notorious instability in aqueous media.[10] One of the solutions is to construct a metal-insulator-semiconductor (MIS) structure;[11] the passivation of Si with its native silicon oxide (SiO_x) can protect to some extent the photoanode from the corrosive environment whereas a coating of an OER-active metal can enhance the catalytic activity.[12] Another crucial benefit of this structure is the creation of a Schottky barrier; the resulting band-bending increases the built-in voltage and subsequently the photovoltage upon illumination which can reduce the external bias needed to drive the reactions.[13] For n-type Si photoanodes, a high-work function metal is required to induce a large Schottky barrier; however, OER-active metals possess moderate work function (ϕ) for the purpose [e.g., ϕ(Fe) = 4.8 eV; ϕ(Co) = 5.0 eV; and ϕ(Ni) = 5.2 eV].[14,15]

Beyond the standard MIS interface, increased inhomogeneity of the metal layer, e.g., through the top-down PEC dissolution, can further enhance the PEC performance.[16,17] This modification introduces a new junction between n-Si and an oxidized phase of the base metal which has a larger work function and thus a larger Schottky barrier. Surrounding a MIS junction by another one with a larger barrier develops a pinch-off region, further increasing the photovoltage.[18] Another route to directly construct inhomogeneous n-Si/SiO_x/M (M = Co, Ni, or Fe)[19–21] MIS structures is the bottom-up electrodeposition method which is simple and cost-

effective. The cathodic deposition allows the simultaneous coating of metal nanoparticles (NPs) and an amorphous SiO_x tunnel layer with a thickness of a few nanometers.[19,21,22] Similar to the top-down approach, the surrounding layer of the base metal is generally its oxidized phase, such as oxide,[23] hydroxide,[24] or oxyhydroxide.[19,22] However, if the surrounding layer can be modified to other compounds with a higher work function, the pinch-off effect and the resulting photovoltage will be larger, improving the PEC performance further. To this end, coordination polymers (CPs), such as metal-organic frameworks (MOFs) and Prussian blue analogs, are emerging as a new class of semiconductors that can be applied as the surrounding layer.[25–28] CPs are recently gaining a great deal of attention due to their facile synthesis, versatile structural designs, and highly tunable properties.[29,30] Herein, we employ copper(I) thiocyanate (CuSCN), a transparent p-type CP semiconductor, to construct a $Si/SiO_x/Cu/CuSCN$ MIS structure via simple solution-based methods to obtain a new photoanode structure with a large photovoltage.

Earth-abundant Cu, recognized as an OER-active material,[31–33] can be used as a substrate for a simple chemical deposition CuSCN.[34] The latter is a 3D coordination polymer consisting of Cu(I) centers bridged by SCN^- ligands.[35] In the past decade, CuSCN has emerged as a technologically important p-type semiconductor with extensive applications as a transparent p-type channel or hole-transport layer (HTL) in various devices, such as thin film transistors,[36,37] organic photovoltaics,[38,39] organic light-emitting diodes,[40] perovskite solar cells,[41,42] and oxide-based photoelectrodes.[43] The basis for the success of CuSCN is attributed to its excellent optical transparency in the visible region and good hole mobility (>0.01 $cm^2\ V^{-1}\ s^{-1}$).[35] Because Cu and CuSCN have work functions of 4.5-4.9 eV[44] and 5.4 eV,[37,45] respectively, the coexistence of Cu and CuSCN on the n-Si surface is expected to develop a strong pinch-off effect and increase the PEC performance. The large band gap of CuSCN (>3.5 eV)[35] also means that the coating will not lead to parasitic absorption that would otherwise decrease the visible light reaching the Si absorber. In this work, electrodeposition and chemical deposition methods were employed to coat Cu and CuSCN, respectively, on the n-Si surface. The resulting $n\text{-}Si/SiO_x/Cu/CuSCN$ photoanode

yields a large photovoltage of 460 mV and a large effective barrier height of 1.03 eV. Additionally, we compare the results with n-Si/SiO_x/Cu structured by the top-down PEC dissolution approach. The latter method can also significantly improve the PEC performance by increasing the inhomogeneity of the planar Cu layer and partially forming CuO_x. Even then, the n-Si/SiO_x/Cu/CuSCN from the bottom-up approach still shows superior performance with the lowest onset potential of 1.27 V vs RHE amongst the photoanodes studied in this work.

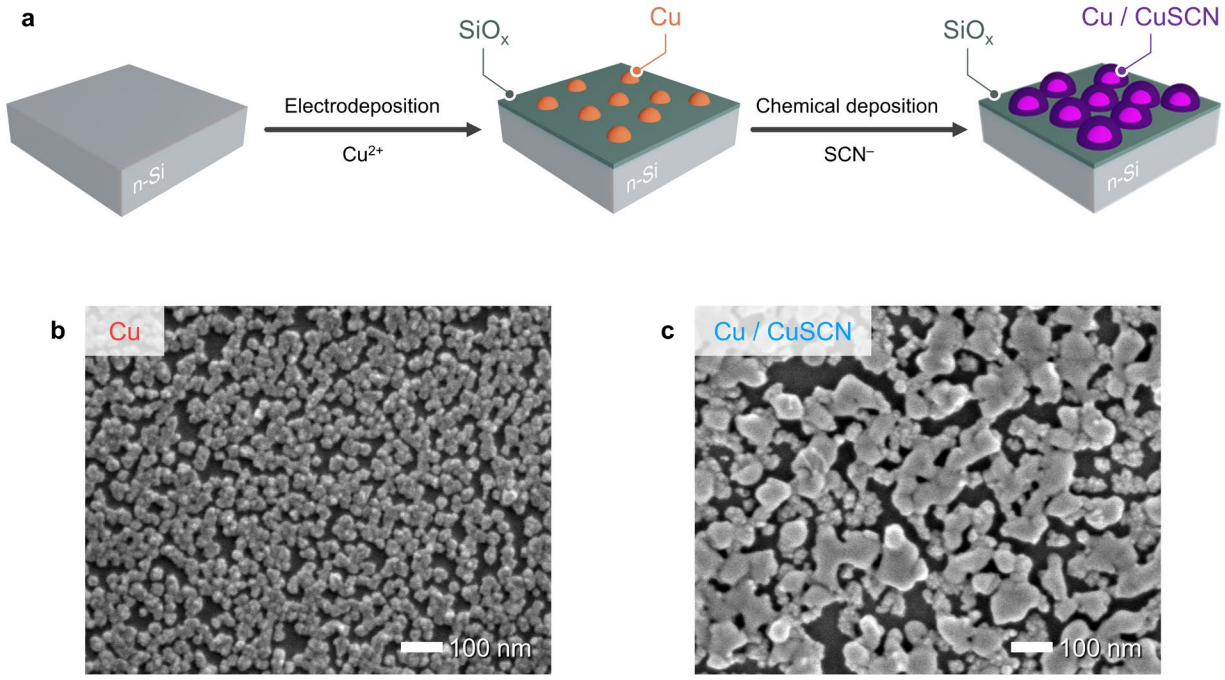

Figure 1. (a) Schematic of the preparation process for n-Si/SiO_x/Cu/CuSCN MIS photoanode prepared successively by electrodeposition and chemical bath deposition methods. SEM images of (b) n-Si/SiO_x/Cu-200s and (c) n-Si/SiO_x/Cu/CuSCN-5s.

To prepare the n-Si/SiO_x/Cu MIS electrode, Cu was first electrodeposited (Figure 1a) on freshly etched n-Si (100) from an aqueous solution containing 2 mM copper(II) sulfate and 10 mM sodium citrate (pH adjusted to 3 with H_2SO_4). The full experimental procedures are included in Note S1 (Supporting Information, SI). We applied two-step cathodic potentials of -1.0 V vs

Ag/AgCl for 0.5 s and successively -0.5 V vs Ag/AgCl for varying amount of time to seed and grow Cu NPs, respectively (chronoamperometric plot shown in Figure S1). The second potential step also allows the growth of an amorphous SiO_x interlayer,[46] creating the MIS structure. The electrodeposition time of the latter was varied from 50 to 300 s, and the samples are labeled as "n-Si/SiO_x/Cu-t_{el}", with t_{el} corresponding to the electrodeposition time in seconds. As discussed next, the n-Si/SiO_x/Cu-200s photoanode yielded the best PEC performance and was employed in the subsequent step of coating CuSCN.

The n-Si/SiO_x/Cu-200s sample was then dipped in an aqueous bath containing 10 mM ammonium thiocyanate and 10 mM ethylenediaminetetraacetic disodium salt (EDTA, measured pH = 4.7) without stirring. The chemical deposition time was varied between 0 and 60 s. The samples after this step are designated as "n-Si/SiO_x/Cu/CuSCN-t_{ch}", with t_{ch} corresponding to the chemical deposition time in seconds. Also based on the PEC performance as shown next, the optimal t_{ch} was 5 s. The successful formation of Cu and Cu/CuSCN layers was corroborated by X-ray photoelectron spectroscopy (XPS), Raman spectroscopy, and optical reflectance spectroscopy as discussed in detail in Note S2 with the data presented in Figure S2 and S3. The resulting film morphology was observed with scanning electron microscopy (SEM), and Figure 1b shows the image of n-Si/SiO_x/Cu-200s. The mean diameter of Cu NPs for this condition was 30±5 nm with a 72% surface coverage. With the increasing t_{el} from 50 to 300 s, the average diameter and surface coverage increased (Figure S4). After the chemical deposition of CuSCN, randomly-dispersed and nonuniform particles appeared as shown in Figure 1c for n-Si/SiO_x/Cu/CuSCN-5s. Prolonging the chemical deposition further, CuSCN predominantly covered the substrate while the number density and size of Cu NPs significantly decreased (Figure S5).

The PEC performance of all electrodes was tested in a moderate alkaline condition of Li-borate/K-borate buffer, measured pH = 9.6. The borate buffer was chosen because it can extend the photoanode lifetime during OER.[12,21,31] Figure 2a and b show the results from cyclic

voltammetry (CV) obtained for the n-Si/SiO_x/Cu-t_{el} and n-Si/SiO_x/Cu/CuSCN-t_{ch} photoanodes, respectively, in the dark and under illumination by simulated AM1.5G sunlight at 1 sun intensity. For all n-Si/SiO_x/Cu electrodes under illumination, the onset potentials (to produce a photocurrent density of 1 mA cm^{-2}) were >140 mV relative to $E^0_{O_2/H_2O}$. The best photoanode was n-Si/SiO_x/Cu-200s which exhibited the lowest onset potential. This condition was therefore used in the subsequent step of CuSCN deposition as mentioned earlier.

After n-Si/SiO_x/Cu-200s was coated with CuSCN, the onset potential was negatively shifted to ~40 and ~50 mV relative to $E^0_{O_2/H_2O}$ for t_{ch} = 5 and 30 s, respectively (Figure 2b). A longer deposition time resulted in reduced performance as observed for n-Si/SiO_x/Cu/ CuSCN-60s. We also performed the dark/light open-circuit potential (OCP) measurements in a solution containing of 5/5 mM ferri/ferrocyanide and 1 M KCl (Figure S6). The photovoltage can be calculated from the difference in the OCP values before and during illumination. In Figure 2c, the photovoltage of n-Si/SiO_x/Cu/CuSCN-t_{ch} shows a similar trend with their PEC performance. Comparing the n-Si/SiO_x/Cu/CuSCN-0s photoanode (i.e., without the CuSCN layer) and n-Si/SiO_x/Cu/CuSCN-5s, the photovoltage increased substantially from 270 to 460 mV. The larger photovoltage measured from OCP may suggest that the coating evolves during the anodic reaction. As discussed later, this is likely due to the instability of Cu and Cu(I) species.

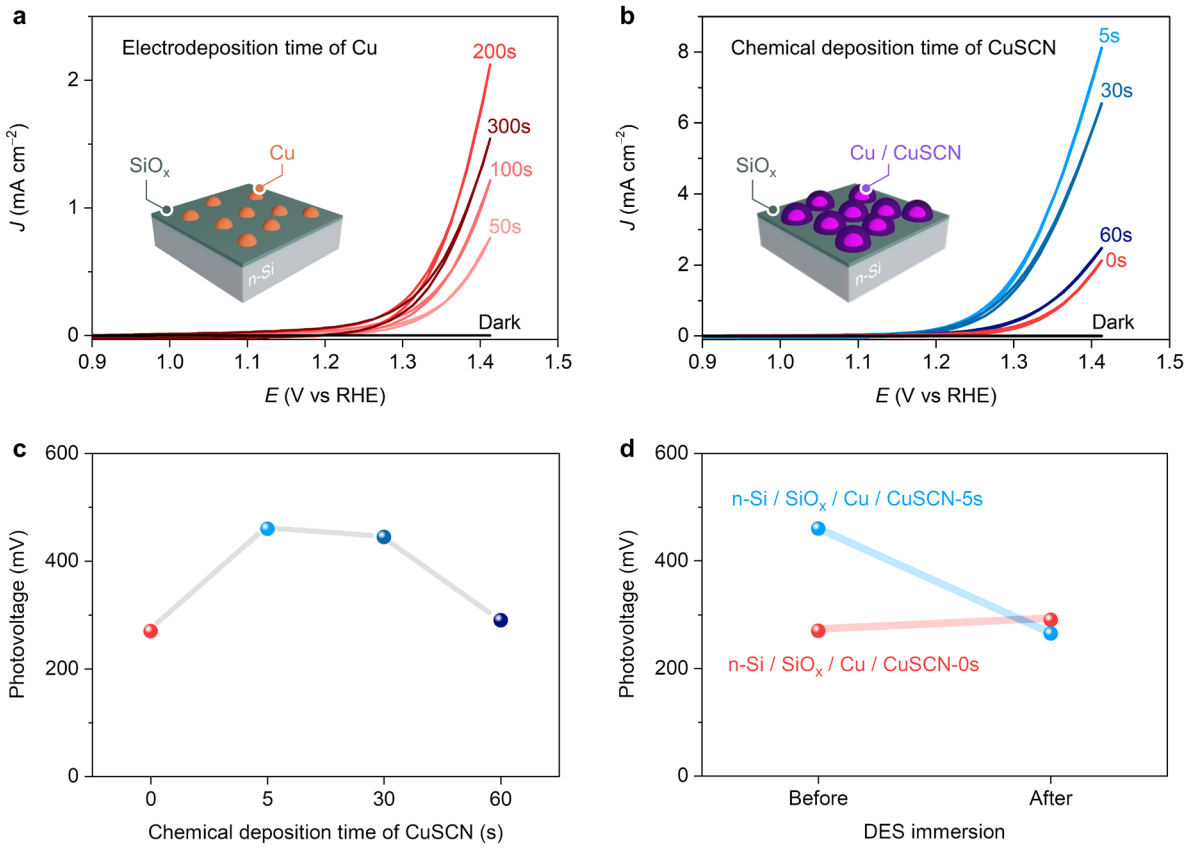

Figure 2. Cyclic voltammograms recorded under simulated sunlight of (a) n-Si/SiO_x/Cu with varying electrodeposition time and (b) n-Si/SiO_x/Cu/CuSCN with varying chemical deposition time. All measurements were conducted in Li-borate/K-borate buffer at a scan rate of 100 mV s^{-1}. (c) Photovoltage of n-Si/SiO_x/Cu/CuSCN as a function of the chemical deposition time. (d) Photovoltage of n-Si/SiO_x/Cu/CuSCN and n-Si/SiO_x/Cu before and after immersing in diethyl sulfide (DES). All photovoltage values were determined by dark/light OCP measurements in a solution containing 5/5 mM ferri/ferrocyanide and 1 M KCl.

To verify the significance of CuSCN on the photovoltage enhancement, selective removal of CuSCN was carried out using diethyl sulfide (DES) as the solvent.[37] A decrease in the photovoltage was expected upon the removal of the surrounding high work function layer.[18] After soaking in DES, the SEM image (Figure S7) shows that the original CuSCN particles vanished.

Some fibrous residue, which was probably formed by other Cu complexes, such as $[Cu(SCN)(DES)]_n$,[37,47] remained on the substrate. The OCP measurements were then carried out again for n-Si/SiO_x/Cu/CuSCN-5s and n-Si/SiO_x/Cu/CuSCN-0s (i.e., Cu only, as a control) after soaking in DES for 5 min (Figure S8). As summarized in Figure 2d, the photovoltage of n-Si/SiO_x/Cu/CuSCN clearly dropped back to a value similar to that of fresh n-Si/SiO_x/Cu following the DES immersion. Conversely, the change in the photovoltage of the control sample was negligible. This result hence corroborates that the photovoltage enhancement arises from the presence of CuSCN. In addition, by comparing the OER activity between non-photoactive FTO/Cu and FTO/CuSCN (Figure S9), we can identify that Cu serves as an OER electrocatalyst whereas CuSCN indeed only affects the interfacial energetics.

Further investigations of the two optimal conditions (t_{el} = 200 s for Cu-only and t_{ch} = 5 s for Cu/CuSCN) are discussed hereafter. Solid-state measurements were performed to examine the interfacial energetics of the MIS nanojunction (see SI for more details). In Figure 3a, the current-voltage curves of the optimal n-Si/SiO_x/Cu and n-Si/SiO_x/Cu/CuSCN solid-state cells clearly exhibit the rectifying behavior of a Schottky junction. When a positive voltage (V > 0) is applied from the n-Si side, i.e., a reverse bias condition, the bands bend downward, thus increasing the potential barrier and suppressing the flow of electrons to the Cu or Cu/CuSCN contact.[48] Under this operating condition, wherein n-Si near the junction is in the depletion regime, n-Si/SiO_x/Cu/CuSCN showed an extremely low current density on the order of μA cm^{-2}, compared to ~mA cm^{-2} of n-Si/SiO_x/Cu. The superior electron-blocking behavior of the optimized electrode can be attributed to the high conduction band level of CuSCN formed by the π* state of the ligand.[49] In addition, the CuSCN junction also creates a larger barrier as discussed next.

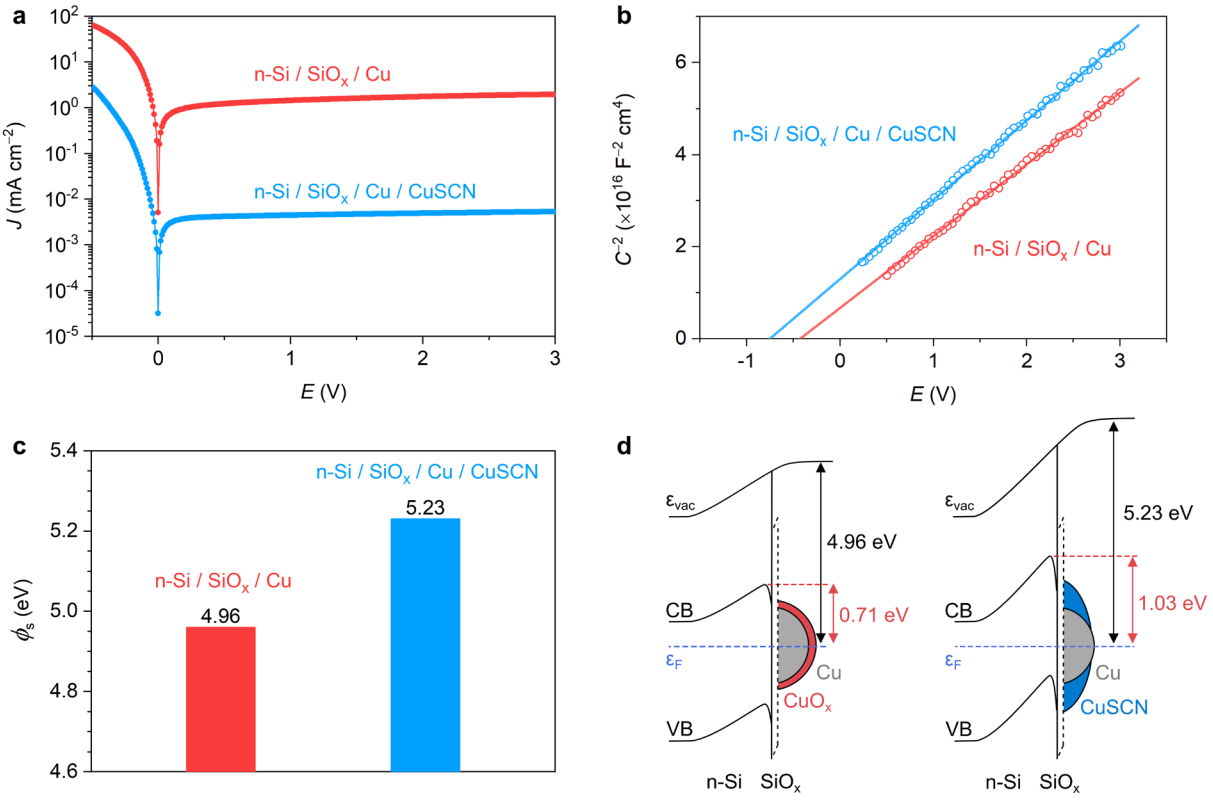

Figure 3. (a) Current density-voltage characteristics and (b) Mott-Schottky plots from solid-state measurements. (c) Surface work function (ϕ_s) from Kelvin Probe measurements. (d) Schematic energy band diagrams of n-Si/SiO$_x$/Cu (red) and n-Si/SiO$_x$/Cu/CuSCN (blue) showing the effective barrier heights (ϕ_b) of 0.71 and 1.03 eV, respectively.

The Mott-Schottky analysis of the solid-state devices was conducted to determine the effective barrier height.[19] Capacitance-voltage measurements were recorded in the depletion regime (reverse bias) with an AC frequency of 100 kHz. As shown in Figure 3b, the flat-band potentials (E_{fb}) can be obtained from the extrapolated *x*-axis intercepts as: -0.44 and -0.76 V for n-Si/SiO$_x$/Cu and n-Si/SiO$_x$/Cu/CuSCN, respectively. The slopes of the fitting lines yield a doping concentration of ~7-8×10^{14} cm^{-3} for both electrodes, corresponding to a resistivity of ~5 Ω·cm, agreeing with the range specified by the Si wafer manufacturer. The effective barrier heights (ϕ_b) of n-Si/SiO$_x$/Cu and n-Si/SiO$_x$/Cu/CuSCN were 0.71 and 1.03 eV, respectively (see calculation

details in SI). We remark that ϕ_b of the optimized electrode with CuSCN is larger than ϕ_b of other inhomogeneous MIS junctions reported in the literature with values in the range of 0.75-0.91 eV.[16,17,19]

The surface work functions (ϕ_s) of n-Si/SiO_x/Cu and n-Si/SiO_x/Cu/CuSCN can be obtained from Kelvin probe measurements. We found that the contact potential difference (CPD) of n-Si/SiO_x/Cu/CuSCN was ~270 mV higher than that of n-Si/SiO_x/Cu (Figure S10a). ϕ_s was calculated with respect to the work function of an Au reference measured by photoelectron yield spectroscopy (PYS, Figure S10b). As summarized in Figure 3c, ϕ_s of n-Si/SiO_x/Cu/CuSCN was 5.23 eV, which is higher than 4.96 eV found for n-Si/SiO_x/Cu. An increase in the surface work function for n-Si/SiO_x/Cu/CuSCN relative to n-Si/SiO_x/Cu is in accordance with the larger effective barrier height, indicating a significant improvement of the band bending characteristics at the MIS interface. By combining ϕ_b and ϕ_s , we can construct the energy band diagrams for n-Si/SiO_x/Cu and n-Si/SiO_x/Cu/CuSCN as shown in Figure 3d.[18,50,51] As discussed in SI (Note S3 and Figure S11-S13), we also studied the stability of our photoanodes and found that they suffered some instability mostly due to Cu corrosion. Cu(I) centers in CuSCN may also undergo undesirable redox reactions during OER as evident from the difference in the photovoltage observed in CV and OCP measurements. Further work is required to resolve the stability issue, for example by alloying Cu with other transition metals[52] or modifying the electrolyte.[53,54]

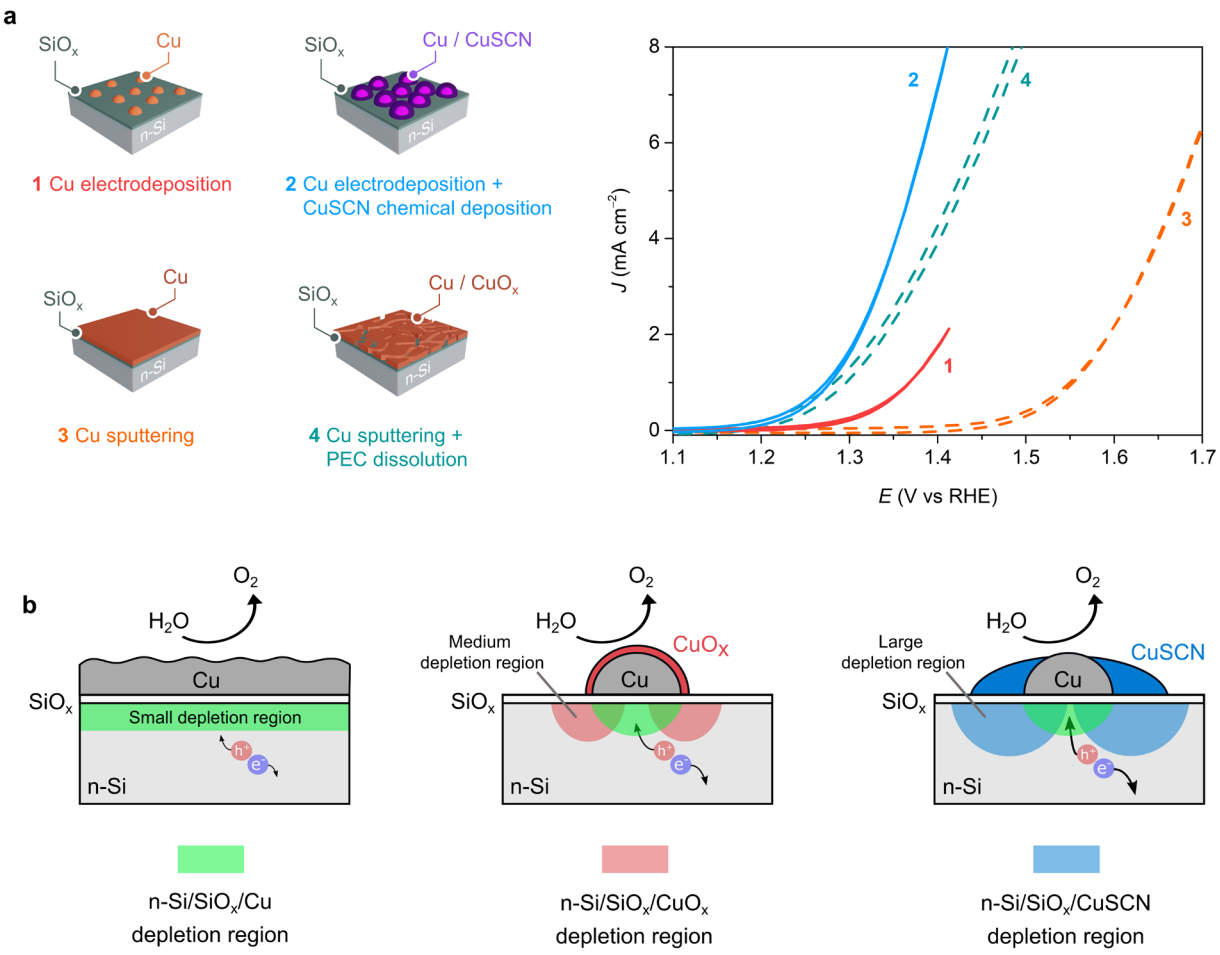

Figure 4. (a) Schematic diagrams of different Cu-modified n-Si photoanodes investigated in this work and their corresponding OER cyclic voltammograms (sample conditions are designated by number and color). All electrodes were measured under simulated sunlight in Li-borate/K-borate buffer solution (pH 9.6). (b) Schematic diagrams illustrating the depletion regions produced by (left) a planar Schottky contact and (center and right) contacts with the pinch-off effect. A small depletion region introduced by the Cu base metal creates a small Schottky barrier, leading to low electron/hole selectivity. The appearances of CuO_x and CuSCN surrounding the base metal create medium and large depletion regions, respectively, resulting in the pinch-off effect and an increase in the electron/hole selectivity.

In addition, we also compared the n-Si/SiO_x/Cu/CuSCN electrode with an inhomogeneous MIS junction based on Cu, i.e., n-Si/SiO_x/Cu electrode prepared by the top-down PEC dissolution approach. So far, this method has been demonstrated only for the Ni-based MIS structure and found to enhance the PEC performance due to the pinch-off effect.[16,17,55] Herein, we sputtered a 25-nm Cu layer on a chemically oxidized n-Si/SiO_x surface to obtain an initially homogeneous MIS junction. Following that, the as-sputtered electrode was activated by running multiple CV cycles between 0.9 and 1.8 V vs RHE in the Li-borate/K-borate buffer under simulated sunlight. As shown in Figure S14, the current density increased with the number of cycles and reached the highest value after 35 cycles, after which the current dramatically dropped. SEM images (Figure S15) show that the sputtered Cu layer contained a large density of cracks upon the PEC dissolution. The XPS analysis (Note S4 and Figure S16) confirmed the presence of CuO_x after the modification. Thus, the performance improvement can be attributed to the formation of the inhomogeneous MIS junction as well as the formation of the CuO_x surrounding layer, similar to the case of Ni-based MIS electrodes (in which the surrounding layer is NiOOH).[16,17,18]

Figure 4a summarizes the PEC performance of all Cu-based MIS photoanodes as reported in this work with the schematics of the pinch-off effect illustrated in Figure 4b. Compared to the flat and homogeneous n-Si/SiO_x/Cu (from sputtering), the PEC dissolution method can dramatically improve the performance, shifting the onset potential from 1.55 to 1.28 V vs RHE. Depositing Cu nanoparticles using the bottom-up electrodeposition also lowers the onset potential to 1.36 V vs RHE, and this can be further improved by chemically converting Cu to CuSCN. The photoanode with the highest performance in this work is n-Si/SiO_x/Cu/CuSCN with the onset potential of 1.27 V vs RHE. For the homogeneous MIS interface, only a small depletion region is formed by the presence of Cu. When the metal is downsized to nanoscale and surrounded by its oxidized phase CuO_x or the high-work function CuSCN, medium and large depletion regions are formed, respectively. The depletion region of the surrounding layer overlaps with that of the base

metal, creating the pinch-off region. The latter leads to higher electron/hole selectivity, which suppresses the charge recombination and thus enhances the photovoltage.[18]

In conclusion, we demonstrate a simple and cost-effective bottom-up chemical deposition method for the preparation of an efficient MIS nanojunction. Surrounding the n-Si/SiO_x/Cu contact with the high-work function CuSCN results in favorable interfacial energetics with a large barrier height, significantly improving the photovoltage and the PEC performance. Besides, the top-down PEC dissolution method is also demonstrated to be effective at enhancing the PEC performance of a planar structure by increasing the inhomogeneity and partially forming CuO_x. The improvement mechanism of both methods can be explained based on the pinch-off effect. CuSCN is highly promising due to its large work function and excellent electron-blocking property. Its large band gap also leads to excellent optical transparency whereas other surrounding layers (CoOOH, NiOOH, or CuO_x) are strongly colored. The transparent CuSCN coating allows the modification of the interfacial energetics without reducing the amount of light reaching the Si photoelectrode. Our findings open new avenues for developing MIS photoelectrodes through the facile use of structurally diverse coordination polymers.

AUTHOR INFORMATION

Corresponding Author

*Pichaya Pattanasattayavong, e-mail: pichaya.p@vistec.ac.th

ORCID

Ponart Aroonratsameruang: 0000-0002-3519-0444

Kanokwan Klahan: 0000-0003-2345-1632

Gabriel Loget: 0000-0003-4809-5013

Pichaya Pattanasattayavong: 0000-0001-6374-1840

Notes

The authors declare no competing financial interests.

ACKNOWLEDGMENT

P.A., K.K. and P.P. would like to acknowledge the funding from Vidyasirimedhi Institute of Science and Technology (VISTEC) and support of scientific instruments from VISTEC's Frontier Research Center (FRC). This project is funded by Thailand Science Research and Innovation (TSRI), grant no. FRB650023/0457, and National Research Council of Thailand (NRCT), grant no. N42A650254. S. Ittisanronnachai is acknowledged for their help with XPS measurements.

REFERENCES

(1) Hemmerling, J. R.; Mathur, A.; Linic, S. Design Principles for Efficient and Stable Water Splitting Photoelectrocatalysts. *Acc. Chem. Res.* **2021**, *54* (8), 1992–2002. https://doi.org/10.1021/acs.accounts.1c00072.

(2) Jin, S. What Else Can Photoelectrochemical Solar Energy Conversion Do Besides Water Splitting and CO_2 Reduction? *ACS Energy Lett.* **2018**, *3* (10), 2610–2612. https://doi.org/10.1021/acsenergylett.8b01800.

(3) Mefford, J. T.; Akbashev, A. R.; Kang, M.; Bentley, C. L.; Gent, W. E.; Deng, H. D.; Alsem, D. H.; Yu, Y.-S.; Salmon, N. J.; Shapiro, D. A.; et al. Correlative Operando Microscopy of Oxygen Evolution Electrocatalysts. *Nature* **2021**, *593* (7857), 67–73. https://doi.org/10.1038/s41586-021-03454-x.

(4) Nong, H. N.; Falling, L. J.; Bergmann, A.; Klingenhof, M.; Tran, H. P.; Spöri, C.; Mom, R.; Timoshenko, J.; Zichittella, G.; Knop-Gericke, A.; et al. Key Role of Chemistry versus Bias

in Electrocatalytic Oxygen Evolution. *Nature* **2020**, *587* (7834), 408–413. https://doi.org/10.1038/s41586-020-2908-2.

(5) Zeng, G.; Pham, T. A.; Vanka, S.; Liu, G.; Song, C.; Cooper, J. K.; Mi, Z.; Ogitsu, T.; Toma, F. M. Development of a Photoelectrochemically Self-Improving Si/GaN Photocathode for Efficient and Durable H_2 Production. *Nat. Mater.* **2021**. https://doi.org/10.1038/s41563-021-00965-w.

(6) Gurudayal, G.; Beeman, J. W.; Bullock, J.; Wang, H.; Eichhorn, J.; Towle, C.; Javey, A.; Toma, F. M.; Mathews, N.; Ager, J. W. Si Photocathode with Ag-Supported Dendritic Cu Catalyst for CO_2 Reduction. *Energy Environ. Sci.* **2019**, *12* (3), 1068–1077. https://doi.org/10.1039/C8EE03547D.

(7) Kempler, P. A.; Richter, M. H.; Cheng, W.-H.; Brunschwig, B. S.; Lewis, N. S. Si Microwire-Array Photocathodes Decorated with Cu Allow CO_2 Reduction with Minimal Parasitic Absorption of Sunlight. *ACS Energy Lett.* **2020**, *5* (8), 2528–2534. https://doi.org/10.1021/acsenergylett.0c01334.

(8) Peramaiah, K.; Ramalingam, V.; Fu, H.; Alsabban, M. M.; Ahmad, R.; Cavallo, L.; Tung, V.; Huang, K.; He, J. Optically and Electrocatalytically Decoupled Si Photocathodes with a Porous Carbon Nitride Catalyst for Nitrogen Reduction with Over 61.8% Faradaic Efficiency. *Adv. Mater.* **2021**, *33* (18), 2100812. https://doi.org/10.1002/adma.202100812.

(9) Luo, Z.; Wang, T.; Gong, J. Single-Crystal Silicon-Based Electrodes for Unbiased Solar Water Splitting: Current Status and Prospects. *Chem. Soc. Rev.* **2019**, *48* (7), 2158–2181. https://doi.org/10.1039/C8CS00638E.

(10) Zhang, X. G. *Electrochemistry of Silicon and Its Oxide*; Kluwer Academic: Boston, 2001. https://doi.org/10.1007/b100331.

(11) Loget, G. Water Oxidation with Inhomogeneous Metal-Silicon Interfaces. *Curr. Opin. Colloid Interface Sci.* **2019**, *39* (I), 40–50. https://doi.org/10.1016/j.cocis.2019.01.001.

(12) Kenney, M. J.; Gong, M.; Li, Y.; Wu, J. Z.; Feng, J.; Lanza, M.; Dai, H. High-Performance Silicon Photoanodes Passivated with Ultrathin Nickel Films for Water Oxidation. *Science.* **2013**, *342* (6160), 836–840. https://doi.org/10.1126/science.1241327.

(13) Kim, J. H.; Hansora, D.; Sharma, P.; Jang, J.-W.; Lee, J. S. Toward Practical Solar Hydrogen Production – an Artificial Photosynthetic Leaf-to-Farm Challenge. *Chem. Soc. Rev.* **2019**, *48* (7), 1908–1971. https://doi.org/10.1039/C8CS00699G.

(14) Ueda, K.; Shimizu, R. Photoelectric Work Function Study on Iron (100) Surface Combined with Auger Electron Spectroscopy. *Jpn. J. Appl. Phys.* **1973**, *12* (12), 1869–1873. https://doi.org/10.1143/JJAP.12.1869.

(15) Digdaya, I. A.; Trześniewski, B. J.; Adhyaksa, G. W. P.; Garnett, E. C.; Smith, W. A. General Considerations for Improving Photovoltage in Metal-Insulator-Semiconductor Photoanodes. *J. Phys. Chem. C* **2018**, *122* (10), 5462–5471. https://doi.org/10.1021/acs.jpcc.7b11747.

(16) Loget, G.; Mériadec, C.; Dorcet, V.; Fabre, B.; Vacher, A.; Fryars, S.; Ababou-Girard, S. Tailoring the Photoelectrochemistry of Catalytic Metal-Insulator-Semiconductor (MIS) Photoanodes by a Dissolution Method. *Nat. Commun.* **2019**, *10* (1), 1–11. https://doi.org/10.1038/s41467-019-11432-1.

(17) Aroonratsameruang, P.; Pattanasattayavong, P.; Dorcet, V.; Mériadec, C.; Ababou-Girard, S.; Fryars, S.; Loget, G. Structure–Property Relationships in Redox-Derivatized Metal–Insulator–Semiconductor (MIS) Photoanodes. *J. Phys. Chem. C* **2020**, *124* (47), 25907–25916. https://doi.org/10.1021/acs.jpcc.0c08971.

(18) Laskowski, F. A. L.; Oener, S. Z.; Nellist, M. R.; Gordon, A. M.; Bain, D. C.; Fehrs, J. L.; Boettcher, S. W. Nanoscale Semiconductor/Catalyst Interfaces in Photoelectrochemistry. *Nat. Mater.* **2020**, *19* (1), 69–76. https://doi.org/10.1038/s41563-019-0488-z.

(19) Hill, J. C.; Landers, A. T.; Switzer, J. A. An Electrodeposited Inhomogeneous Metal-Insulator-Semiconductor Junction for Efficient Photoelectrochemical Water Oxidation. *Nat. Mater.* **2015**, *14* (11), 1150–1155. https://doi.org/10.1038/nmat4408.

(20) Loget, G.; Fabre, B.; Fryars, S.; Mériadec, C.; Ababou-Girard, S. Dispersed Ni Nanoparticles Stabilize Silicon Photoanodes for Efficient and Inexpensive Sunlight-Assisted Water Oxidation. *ACS Energy Lett.* **2017**, *2* (3), 569–573. https://doi.org/10.1021/acsenergylett.7b00034.

(21) Oh, K.; Dorcet, V.; Fabre, B.; Loget, G. Dissociating Water at N-Si Photoanodes Partially Covered with Fe Catalysts. *Adv. Energy Mater.* **2020**, *10* (3), 1902963. https://doi.org/10.1002/aenm.201902963.

(22) Oh, K.; Mériadec, C.; Lassalle-Kaiser, B.; Dorcet, V.; Fabre, B.; Ababou-Girard, S.; Joanny, L.; Gouttefangeas, F.; Loget, G. Elucidating the Performance and Unexpected Stability of Partially Coated Water-Splitting Silicon Photoanodes. *Energy Environ. Sci.* **2018**, *11* (9), 2590–2599. https://doi.org/10.1039/C8EE00980E.

(23) Lee, S. A.; Lee, T. H.; Kim, C.; Lee, M. G.; Choi, M.-J.; Park, H.; Choi, S.; Oh, J.; Jang, H. W. Tailored NiO_x/Ni Cocatalysts on Silicon for Highly Efficient Water Splitting Photoanodes via Pulsed Electrodeposition. *ACS Catal.* **2018**, *8* (8), 7261–7269. https://doi.org/10.1021/acscatal.8b01999.

(24) Xu, G.; Xu, Z.; Shi, Z.; Pei, L.; Yan, S.; Gu, Z.; Zou, Z. Silicon Photoanodes Partially Covered by Ni@$Ni(OH)_2$ Core-Shell Particles for Photoelectrochemical Water Oxidation.

ChemSusChem **2017**, *10* (14), 2897–2903. https://doi.org/10.1002/cssc.201700825.

(25) M. Pires, B.; Hegner, F. S.; Bonacin, J. A.; Galán-Mascarós, J.-R. Ligand Effects of Penta- and Hexacyanidoferrate-Derived Water Oxidation Catalysts on $BiVO_4$ Photoanodes. *ACS Appl. Energy Mater.* **2020**, *3* (9), 8448–8456. https://doi.org/10.1021/acsaem.0c01082.

(26) Hegner, F. S.; Herraiz-Cardona, I.; Cardenas-Morcoso, D.; López, N.; Galán-Mascarós, J. R.; Gimenez, S. Cobalt Hexacyanoferrate on $BiVO_4$ Photoanodes for Robust Water Splitting. *ACS Appl. Mater. Interfaces* **2017**, *9* (43), 37671–37681. https://doi.org/10.1021/acsami.7b09449.

(27) Beiler, A. M.; McCarthy, B. D.; Johnson, B. A.; Ott, S. Enhancing Photovoltages at P-Type Semiconductors through a Redox-Active Metal-Organic Framework Surface Coating. *Nat. Commun.* **2020**, *11* (1), 5819. https://doi.org/10.1038/s41467-020-19483-5.

(28) Downes, C. A.; Marinescu, S. C. Efficient Electrochemical and Photoelectrochemical H_2 Production from Water by a Cobalt Dithiolene One-Dimensional Metal–Organic Surface. *J. Am. Chem. Soc.* **2015**, *137* (43), 13740–13743. https://doi.org/10.1021/jacs.5b07020.

(29) Alsaç, E. P.; Ülker, E.; Nune, S. V. K.; Dede, Y.; Karadas, F. Tuning the Electronic Properties of Prussian Blue Analogues for Efficient Water Oxidation Electrocatalysis: Experimental and Computational Studies. *Chem. - A Eur. J.* **2018**, *24* (19), 4856–4863. https://doi.org/10.1002/chem.201704933.

(30) Batten, S. R.; Neville, S. M.; Turner, D. R. *Coordination Polymers: Design, Analysis and Application*; Royal Society of Chemistry: Cambridge, 2009. https://doi.org/10.1039/9781847558862.

(31) Shi, Y.; Gimbert-Suriñach, C.; Han, T.; Berardi, S.; Lanza, M.; Llobet, A. CuO-Functionalized Silicon Photoanodes for Photoelectrochemical Water Splitting Devices.

ACS Appl. Mater. Interfaces **2016**, *8* (1), 696–702. https://doi.org/10.1021/acsami.5b09816.

(32) Wang, J.-G.; Shi, L.; Su, Y.; Liu, L.; Yang, Z.; Huang, R.; Xie, J.; Tian, Y.; Li, D. In-Situ Plasmonic Tracking Oxygen Evolution Reveals Multistage Oxygen Diffusion and Accumulating Inhibition. *Nat. Commun.* **2021**, *12* (1), 2164. https://doi.org/10.1038/s41467-021-22434-3.

(33) Zhou, Z.; Li, X.; Li, Q.; Zhao, Y.; Pang, H. Copper-Based Materials as Highly Active Electrocatalysts for the Oxygen Evolution Reaction. *Mater. Today Chem.* **2019**, *11*, 169–196. https://doi.org/10.1016/j.mtchem.2018.10.008.

(34) Xu, J.; Xue, D. Fabrication of Upended Taper-Shaped Cuprous Thiocyanate Arrays on a Copper Surface at Room Temperature. *J. Phys. Chem. B* **2006**, *110* (23), 11232–11236. https://doi.org/10.1021/jp061274x.

(35) Pattanasattayavong, P.; Promarak, V.; Anthopoulos, T. D. Electronic Properties of Copper(I) Thiocyanate (CuSCN). *Adv. Electron. Mater.* **2017**, *3* (3), 1600378. https://doi.org/10.1002/aelm.201600378.

(36) Pattanasattayavong, P.; Yaacobi-Gross, N.; Zhao, K.; Ngonggang Ndjawa, G. O.; Li, J.; Yan, F.; O'Regan, B. C.; Amassian, A.; Anthopoulos, T. D. Hole-Transporting Transistors and Circuits Based on the Transparent Inorganic Semiconductor Copper(I) Thiocyanate (CuSCN) Processed from Solution at Room Temperature. *Adv. Mater.* **2013**, *25* (10), 1504–1509. https://doi.org/10.1002/adma.201202758.

(37) Worakajit, P.; Hamada, F.; Sahu, D.; Kidkhunthod, P.; Sudyoadsuk, T.; Promarak, V.; Harding, D. J.; Packwood, D. M.; Saeki, A.; Pattanasattayavong, P. Elucidating the Coordination of Diethyl Sulfide Molecules in Copper(I) Thiocyanate (CuSCN) Thin Films

and Improving Hole Transport by Antisolvent Treatment. *Adv. Funct. Mater.* **2020**, *30* (36), 2002355. https://doi.org/10.1002/adfm.202002355.

(38) Li, M.; Gao, K.; Wan, X.; Zhang, Q.; Kan, B.; Xia, R.; Liu, F.; Yang, X.; Feng, H.; Ni, W.; et al. Solution-Processed Organic Tandem Solar Cells with Power Conversion Efficiencies >12%. *Nat. Photonics* **2017**, *11* (2), 85–90. https://doi.org/10.1038/nphoton.2016.240.

(39) Yaacobi-Gross, N.; Treat, N. D.; Pattanasattayavong, P.; Faber, H.; Perumal, A. K.; Stingelin, N.; Bradley, D. D. C.; Stavrinou, P. N.; Heeney, M.; Anthopoulos, T. D. High-Efficiency Organic Photovoltaic Cells Based on the Solution-Processable Hole Transporting Interlayer Copper Thiocyanate (CuSCN) as a Replacement for PEDOT:PSS. *Adv. Energy Mater.* **2015**, *5* (3), 1401529. https://doi.org/10.1002/aenm.201401529.

(40) Perumal, A.; Faber, H.; Yaacobi-Gross, N.; Pattanasattayavong, P.; Burgess, C.; Jha, S.; McLachlan, M. A.; Stavrinou, P. N.; Anthopoulos, T. D.; Bradley, D. D. C. High-Efficiency, Solution-Processed, Multilayer Phosphorescent Organic Light-Emitting Diodes with a Copper Thiocyanate Hole-Injection/Hole-Transport Layer. *Adv. Mater.* **2015**, *27* (1), 93–100. https://doi.org/10.1002/adma.201403914.

(41) Ye, S.; Sun, W.; Li, Y.; Yan, W.; Peng, H.; Bian, Z.; Liu, Z.; Huang, C. CuSCN-Based Inverted Planar Perovskite Solar Cell with an Average PCE of 15.6%. *Nano Lett.* **2015**, *15* (6), 3723–3728. https://doi.org/10.1021/acs.nanolett.5b00116.

(42) Arora, N.; Dar, M. I.; Hinderhofer, A.; Pellet, N.; Schreiber, F.; Zakeeruddin, S. M.; Grätzel, M. Perovskite Solar Cells with CuSCN Hole Extraction Layers Yield Stabilized Efficiencies Greater than 20%. *Science.* **2017**, *358* (6364), 768–771. https://doi.org/10.1126/science.aam5655.

(43) Pan, L.; Liu, Y.; Yao, L.; Dan Ren; Sivula, K.; Grätzel, M.; Hagfeldt, A. Cu_2O Photocathodes

with Band-Tail States Assisted Hole Transport for Standalone Solar Water Splitting. *Nat. Commun.* **2020**, *11* (1), 318. https://doi.org/10.1038/s41467-019-13987-5.

(44) Gartland, P. O.; Berge, S.; Slagsvold, B. J. Photoelectric Work Function of a Copper Single Crystal for the (100), (110), (111), and (112) Faces. *Phys. Rev. Lett.* **1972**, *28* (12), 738–739. https://doi.org/10.1103/PhysRevLett.28.738.

(45) Kim, M.; Park, S.; Jeong, J.; Shin, D.; Kim, J.; Ryu, S. H.; Kim, K. S.; Lee, H.; Yi, Y. Band-Tail Transport of CuSCN: Origin of Hole Extraction Enhancement in Organic Photovoltaics. *J. Phys. Chem. Lett.* **2016**, *7* (14), 2856–2861. https://doi.org/10.1021/acs.jpclett.6b01039.

(46) Hull, C. M.; Switzer, J. A. Electrodeposited Epitaxial Cu(100) on Si(100) and Lift-Off of Single Crystal-like Cu(100) Foils. *ACS Appl. Mater. Interfaces* **2018**, *10* (44), 38596–38602. https://doi.org/10.1021/acsami.8b13188.

(47) Ayala, G.; Pike, R. D. Copper(I) Thiocyanate Networks with Aliphatic Sulfide Ligands. *Polyhedron* **2016**, *115*, 242–246. https://doi.org/10.1016/j.poly.2016.05.029.

(48) Neamen, D. A. *Semiconductor Physics and Devices*; McGraw-Hill: New York, 2003.

(49) Jaffe, J. E.; Kaspar, T. C.; Droubay, T. C.; Varga, T.; Bowden, M. E.; Exarhos, G. J. Electronic and Defect Structures of CuSCN. *J. Phys. Chem. C* **2010**, *114* (19), 9111–9117. https://doi.org/10.1021/jp101586q.

(50) Tung, R. T. Electron Transport at Metal-Semiconductor Interfaces: General Theory. *Phys. Rev. B* **1992**, *45* (23), 13509–13523. https://doi.org/10.1103/PhysRevB.45.13509.

(51) Sullivan, J. P.; Tung, R. T.; Pinto, M. R.; Graham, W. R. Electron Transport of Inhomogeneous Schottky Barriers: A Numerical Study. *J. Appl. Phys.* **1991**, *70* (12), 7403–7424. https://doi.org/10.1063/1.349737.

(52) Wang, C.; Sui, Y.; Xiao, G.; Yang, X.; Wei, Y.; Zou, G.; Zou, B. Synthesis of Cu–Ir Nanocages with Enhanced Electrocatalytic Activity for the Oxygen Evolution Reaction. *J. Mater. Chem. A* **2015**, *3* (39), 19669–19673. https://doi.org/10.1039/C5TA05384F.

(53) Du, J.; Chen, Z.; Ye, S.; Wiley, B. J.; Meyer, T. J. Copper as a Robust and Transparent Electrocatalyst for Water Oxidation. *Angew. Chemie* **2015**, *127* (7), 2101–2106. https://doi.org/10.1002/ange.201408854.

(54) Tennakone, K.; Shantha Pushpa, G. S.; Punchihewa, S.; Epa, G. Stability of Cuprous Thiocyanate Coated Cuprous Oxide Photocathode in Aqueous Thiocyanate. *Electrochim. Acta* **1986**, *31* (3), 315–318. https://doi.org/10.1016/0013-4686(86)80084-6.

(55) Laskowski, F. A. L.; Nellist, M. R.; Venkatkarthick, R.; Boettcher, S. W. Junction Behavior of N-Si Photoanodes Protected by Thin Ni Elucidated from Dual Working Electrode Photoelectrochemistry. *Energy Environ. Sci.* **2017**, *10* (2), 570–579. https://doi.org/10.1039/C6EE03505A.